View metadata, citation and similar papers at core.ac.uk

brought to you by CORE

provided by Explore Bristol Research

Yajima, T., Minohara, M., Bell, C., Hwang, H. Y., & Hikita, Y. (2018). Inhomogeneous barrier heights at dipole-controlled $SrRuO_3$/Nb:$SrTiO_3$ Schottky junctions. *Applied Physics Letters*, *113*(22), [221603]. https://doi.org/10.1063/1.5052712

Peer reviewed version

Link to published version (if available):
10.1063/1.5052712

Link to publication record in Explore Bristol Research
PDF-document

This is the author accepted manuscript (AAM). The final published version (version of record) is available online via AIP at https://aip.scitation.org/doi/10.1063/1.5052712 . Please refer to any applicable terms of use of the publisher.

University of Bristol - Explore Bristol Research

General rights

This document is made available in accordance with publisher policies. Please cite only the published version using the reference above. Full terms of use are available: http://www.bristol.ac.uk/pure/about/ebr-terms

Inhomogeneous barrier heights at dipole-controlled $SrRuO_3$ / Nb:$SrTiO_3$ Schottky junctions

T. Yajima,[1,2,a)] M. Minohara,[2,3] C. Bell,[2,4] H. Y. Hwang,[2,5] and Y. Hikita,[2,a)]

[1]*Department of Materials Engineering, The University of Tokyo, Tokyo 113-8656, Japan*

[2]*Stanford Institute for Materials and Energy Sciences, SLAC National Accelerator Laboratory, Menlo Park, California 94025, USA*

[3]*Electronics and Photonics Research Institute, National Institute of Advanced Industrial Science and Technology, Tsukuba, Ibaraki 305-8568, Japan*

[4]*H. H. Wills Physics Laboratory, University of Bristol, Tyndall Avenue, Bristol, BS8 1TL, UK*

[5]*Geballe Laboratory for Advanced Materials, Department of Applied Physics, Stanford University, Stanford, California 94305, USA*

It has recently been shown that the Schottky barrier height (SBH) formed at metal-semiconductor perovskite oxide heterojunctions can be dramatically tuned by the insertion of atomic-scale dipole layers at the interface. However, in idealized form, this would only allow for specific values of the SBH, discretized by the dipole layer thickness. Here we examine the effect of fractional unit cell $LaAlO_3$ dipoles inserted between $SrRuO_3$ and Nb:$SrTiO_3$ in (001) Schottky junctions, as a function of their in-plane lateral distribution. When the $LaAlO_3$ dipoles are finely dispersed, we observe uniformly rectifying junctions, with SBHs reflecting the fractional $LaAlO_3$ coverage. For larger length-scale distributions, the junction characteristics reflect the inhomogeneous combination of regions with and without the interface dipole. The characteristic length scale dividing the two regimes corresponds to the semiconductor depletion width scaled by the dipole potential, determining the effective scale for which the SBH can be continuously tuned.

a)Authors to whom correspondence should be addressed. Electronic mail: yajima@adam.t.u-tokyo.ac.jp and hikita@stanford.edu.

Complex oxides are targeted as constituents of various electronic,[1] electrochemical,[2] electromechanical,[3] and optoelectronic devices,[4] due to their wide range of physical and chemical properties which can be controlled by external stimuli such as electric field, light, and mechanical stress. In order to effectively implement these materials functionalities in devices, it is critical to develop techniques to engineer interface band alignments, which determine the carrier transport across solid or solid/liquid interfaces. In many materials, interface band alignments are generally determined by the bulk properties of the two constituents, with limited ability to manipulate them.[5] However, in atomic-scale complex oxide heterostructures, it has been found that band alignments can be significantly modulated by artificially creating interface dipoles in Schottky junctions and at oxide/liquid interfaces, and has shown great potential as a powerful device technique. [6-12]

The underlying principle of dipole engineering relies on atomistically positioning a pair of positive and negative charge layers, which create the extra potential to effectively modify the interface band alignment. Ultrathin layers of perovskite oxides are ideal materials for forming such dipole layers because their crystal structure inherently has the flexibility to host charged atomic layers along a certain orientation by appropriate selection of the two cations. A representative example is the use of ultrathin $LaAlO_3$ layers parallel to the (001) plane, forming a $(AlO_2)^-/(LaO)^+$ stack. When inserted between charge neutral TiO_2-terminated (001)-oriented Nb-doped $SrTiO_3$ (Nb:$SrTiO_3$) and $SrRuO_3$ (001) surfaces, the rectifying Schottky junction is converted into an Ohmic contact.[8] Here, Nb:$SrTiO_3$ is the *n*-type semiconductor substrate and $SrRuO_3$ is the metal layer epitaxially deposited above the $(AlO_2)^-/(LaO)^+$ dipole layer [Fig. 1(a)]. The strong ionicity of perovskites, combined with the ability to form atomically well-defined and coherent interfaces, enabled band alignment modulation on the order of 1 V per perovskite unit cell (uc), providing an unprecedented range of tunability in any semiconductor/metal system.[13, 14] Despite its effectiveness in increasing the photovoltage in Schottky photodiodes[12] and reducing junction resistance with high dielectric constant semiconductors,[15, 16] the huge electric field

induced between the atomic layers demands delicate control of the dipole layer. In particular, sub-unit cell thickness control is required to practically achieve precise tuning of barrier heights on the scale of 10 - 100 meV. For perovskite oxides, sub-unit cell thickness corresponds to single-unit cell-thick islands covering a fractional area over the surface [Fig. 1(b)], which naturally leads to the question of how the lateral size of the nanoscale dipole islands influence the potential profile and the associated macroscopic junction properties.

Here, we take archetypal $SrRuO_3$/Nb:$SrTiO_3$ (001) Schottky junctions,[17, 18] engineered with a $(AlO_2)^-/(LaO)^+$ dipole layer, to study the lateral size effect of the fractional dipole islands on the macroscopic current-voltage (*I*-*V*) characteristics. For relatively small dipole islands, a systematic reduction in the Schottky barrier height (SBH) is observed while maintaining macroscopic lateral uniformity. On the other hand, the junction characteristics are clearly inhomgeneous for relatively large dipole islands, strongly deviating from the ideal thermionic emission model. The characteristic length scale dividing the two regimes corresponds to the semiconductor depletion width scaled by the dipole potential, which we derive from the spatially inhomogeneous Schottky junction model developed by Tung.[19] These results highlight the importance of controlling not only the thickness on the sub-unit cell level, but also the lateral nanostructure dimensions for effective control of oxide interface functionalities.

The epitaxial heterostructures were fabricated using pulsed laser deposition. Prior to deposition, the TiO_2-terminated 0.01 wt. % Nb:$SrTiO_3$ (001) substrate was pre-annealed at 950 ^{o}C under a partial oxygen pressure P_{O2} of 5×10^{-5} Torr for 30 min to obtain sharp atomic step-terrace structure. The dipole layer was formed by depositing 0 – 2 uc of $LaAlO_3$ at $P_{O2} = 1 \times 10^{-5}$ Torr and laser fluence $F = 1.5$ Jcm^{-2}, followed by the growth of a 20-nm thick $SrRuO_3$ thin film at substrate temperature $T_s = 750$ ^{o}C, $P_{O2} = 0.3$ Torr, and $F = 3$ Jcm^{-2}. The thickness of the $LaAlO_3$ layer was controlled by using reflection high-energy electron diffraction oscillations as well as growth rate calibration using laser pulse counts. The lateral size of the dipole islands was controlled by varying T_s between 750 ^{o}C to 1100 ^{o}C to access layer-

by-layer and step-flow growth modes.[20] The fabricated structures were patterned into multiple 0.22 mm-diameter circular electrodes by Ar^+-ion milling of the deposited layers followed by post-annealing at 350 ^{o}C in P_{O2} = 1 bar for 6 h to fill residual oxygen vacancies. Gold and indium were used as the contact electrodes for the $SrRuO_3$ thin film and the Nb:$SrTiO_3$ (001) substrate, respectively. The surface morphology of the fractionally deposited dipole layers was characterized by atomic force microscopy (AFM) and electrical characterization of the Schottky junctions was conducted using a semiconductor parameter analyzer at room temperature.

Figure 2 shows the AFM images after the growth of 0.4 uc of $LaAlO_3$ on Nb:$SrTiO_3$ (001) substrates under different T_s. At T_s = 750 ^{o}C, several nm-sized islands are vaguely visible on the substrate surface which coalesce at higher T_s [Figs. 2(a) – (c)]. At the highest substrate temperature of T_s = 1100 ^{o}C, the $LaAlO_3$ islands are no longer visible in the topography and a sharp step-terrace structure is recovered [Fig. 2(d)]. By exploiting the force sensitivity to different surface elements in friction force microscopy,[21] we identify that the fractional layers have diffused to the step edges, forming one-dimensional ridges of approximately 200 nm width, exhibiting a clear contrast as shown in Fig. 2(e).

The *I-V* characteristics of the $SrRuO_3$/$LaAlO_3$/Nb:$SrTiO_3$ Schottky junctions with systematically varied $LaAlO_3$ dipole thickness grown at T_s = 750 ^{o}C are shown in Fig. 3(a). The initially rectifying junction exhibited a systematic reduction in the forward bias onset voltage and an increase in the reverse bias current, finally converting into an effectively Ohmic contact at 2 uc insertion, characterized by a symmetric *I-V* curve. Importantly, the *I-V* characteristics followed the typical exponential function under forward bias even for the fractional coverage of the dipoles below 1 uc, indicating electrically homogeneous junction properties with reduced barrier heights, despite the presence of inhomogenously distributed dipole islands at the interface. In contrast, we observe a strong deviation from the simple exponential function for the forward-biased junction with $LaAlO_3$ deposited at T_s = 1100 ^{o}C as shown in Fig. 3(b).

Thus, the dipole-inserted junctions show electrical characteristics determined by both the average dipole thickness and the lateral dipole diameter. When we restrict the average dipole thickness between 0 uc and 1 uc, the junction can be viewed as two different local barrier height (LBH) regions which are laterally distributed with the specific dipole diameter. The simplest model describing such a junction is a linear combination of two independent diodes, assuming the dipole diameter is sufficiently large. Then, the two diodes have different LBHs ($\Phi_{\mathrm{B}}-\Delta$ and Φ_{B}) and area (S_{L} and S_{H}), corresponding to $SrRuO_3/LaAlO_3$/Nb:$SrTiO_3$ (001) and $SrRuO_3$/Nb:$SrTiO_3$ (001), respectively. Φ_{B} is the initial SBH without the dipole island and Δ is the reduction in the LBH due to the presence of the 1 uc $LaAlO_3$ dipole island. Assuming the thermionic emission process for the junction transport,[22] the total current through the electrode I_{total} is given by the sum of the two thermionic emission currents each weighted by their respective area: $I_{\mathrm{total}}=I_0(S_{\mathrm{H}}+S_{\mathrm{L}})\exp(-\beta\overline{\Phi}_{\mathrm{B}}^{\mathrm{LC}})=I_0S_{\mathrm{H}}\exp(-\beta\Phi_{\mathrm{B}})+I_0S_{\mathrm{L}}\exp(-\beta\Phi_{\mathrm{B}}+\beta\Delta)$.[23] Here, $\overline{\Phi}_{\mathrm{B}}^{\mathrm{LC}}$ is the current-averaged SBH in this model, and $\beta=q/k_{\mathrm{B}}T$ and $I_0=A^*T^2(e^{\beta V}-1)$, where, q is the elementary charge, k_{B} is the Boltzmann constant, T is the measurement temperature, A^* is the Richardson constant equal to 156 $\mathrm{Acm^{-2}K^{-2}}$ for Nb:$SrTiO_3$,[24] and V is the applied voltage. The above equation gives a $\overline{\Phi}_{\mathrm{B}}^{\mathrm{LC}}$ logarithmically dependent on $S_{\mathrm{L}}/S_{\mathrm{H}}$, the areal coverage of the islands. I_{total} based on this model is clearly dominated by the lower barrier junction ($\Phi_{\mathrm{B}}-\Delta$) and predicts an abrupt reduction in the measured barrier height with minimal deposition of the dipole layer, not varying further with areal coverage [Fig. 4(a)]. However, this disagrees with the experimentally observed linear dependence, and indicates that the dipole diameter in these junctions is not large enough to treat the two LBH regions independently, and the lateral potential landscape around the perimeters of the low LBH regions needs to be taken into account.

Here, we apply a model of a diode with a LBH of Φ_{B} containing multiple circular islands (diameter d) with low LBHs ($\Phi_{\mathrm{B}}-\Delta$), the area ratio of which is given by $S_{\mathrm{L}}/(S_{\mathrm{H}}+S_{\mathrm{L}})$.[19] First, we

assume d is so small that the two junctions are not independent, but rather form a lateral potential landscape with saddle points under the low LBH regions. The height of the saddle points is approximately given by the area-weighted average of the two LBHs, $\overline{\Phi}_{\mathrm{B}}^{\mathrm{A}} = \frac{S_{\mathrm{H}}\Phi_{\mathrm{B}} + S_{\mathrm{L}}(\Phi_{\mathrm{B}} - \Delta)}{S_{\mathrm{H}} + S_{\mathrm{L}}}$, because the potential is averaged through the lateral band bending and highlights the total inserted dipole moment per area. An example of a calculated potential landscape along a single array of circular dipole islands $V_{\mathrm{B}}(\vec{r})$ is presented in Fig. 4(b) using $V_{\mathrm{B}}(\vec{r}) = V_{\mathrm{bb}}\left(1 - \frac{z}{W}\right)^2 + V_{\mathrm{n}} + V_{\mathrm{comp}} - \sum_{\mathrm{dipole}} \frac{d^2\Delta}{8} \frac{z}{|\vec{r} - \vec{r}_{\mathrm{dipole}}|^{3/2}}$ following ref. 19, where $\vec{r}$ is the coordinate in the semiconductor, z is the interface-perpendicular component of $\vec{r}$, $\vec{r}_{\mathrm{dipole}}$ is the center of each dipole island, $V_{\mathrm{bb}} = \Phi_{\mathrm{B}} - V_{\mathrm{n}}$ is the built-in potential, V_{n} is the energy difference between the conduction band minimum and the Fermi energy, $W = \sqrt{2\varepsilon_0\varepsilon_{\mathrm{S}}V_{\mathrm{bb}}/qN_{\mathrm{D}}}$ is the depletion width, N_{D} is the donor concentration in the semiconductor, ε_0 is the vacuum permittivity, and ε_{S} is the semiconductor relative permittivity. Here, $N_{\mathrm{D}} = 4.4 \times 10^{20}$ cm^{-3}, $\varepsilon_{\mathrm{S}} = 300$, $\Phi_{\mathrm{B}} = 1.35$ eV, $V_{\mathrm{n}} = 0.13$ eV, and $\Delta = 1.0$ eV. We assume circular dipoles with $d = 5$ nm with 10 nm period as shown in the Fig. 4(b) inset, which leads to $S_{\mathrm{L}}/(S_{\mathrm{H}} + S_{\mathrm{L}}) = 0.17$ and $\overline{\Phi}_{\mathrm{B}}^{\mathrm{A}} = 1.18$ eV. The $\overline{\Phi}_{\mathrm{B}}^{\mathrm{A}}$ values reproduce the experimentally measured SBH for the junction with fractional dipole coverage [red dotted line in Fig. 4(a)] as well as the current-voltage characteristics which are calculated based on the thermionic emission model [Fig. 4(d)]. We note that $V_{\mathrm{B}}(\vec{r})$ is offset by $V_{\mathrm{comp}} = S_{\mathrm{L}}\Delta/(S_{\mathrm{H}} + S_{\mathrm{L}})$ in order to compensate for the sum of the potential shift from the superposed dipole islands to realize the equilibrium state: the junction would be in a biased state without V_{comp} far away from the interface.

This calculation clearly shows that the potential close to the interface is reduced by the presence of the lower LBH regions, resulting in an effective SBH given by $\overline{\Phi}_{\mathrm{B}}^{\mathrm{A}}$. It should be noted that the large

variation in the potential close to the interface is diminished far away from the interface as seen in Fig. 4(b). The computed *I-V* characteristics from this potential landscape within the thermionic emission regime is governed by the relative size of the saddle point potential and $\overline{\Phi}_{\mathrm{B}}^{\mathrm{A}}$.[19] When the saddle point potential is close to $\overline{\Phi}_{\mathrm{B}}^{\mathrm{A}}$, the junction shows electrically homogeneous *I-V* characteristics governed by the average SBH and near-unity ideality factor, consistent with the experimental observation in Figs. 4(a) and (c).[19] On the other hand, as the difference between the saddle point potential and $\overline{\Phi}_{\mathrm{B}}^{\mathrm{A}}$ in Fig. 4(b) increases at larger d and larger separation (for a fixed fractional coverage), the junction evolves toward the disappearance of the saddle point (parallel-diode regime), as seen in the *I-V* characteristics for the T_s = 1100 ºC junction. Experimentally for the 1100 ºC junction, even the smallest fractional dipole layer coverage of 0.2 was sufficient to make the *I-V* characteristics symmetric around $V = 0$ and substantially increasing the forward and reverse current, no longer showing the characteristics of a uniform diode [Fig. 3(b)]. In our model, the length scale separating the two *I-V* characteristics is given by the disappearance of a saddle point in band bending. By calculating the condition satisfying $\left(\frac{\partial V_{\mathrm{B}}}{\partial z}\right)_{z=0} < 0$ at the center of the dipole island, the saddle point disappears at $d_{cr} = \frac{\Delta}{\Phi_B} W$. Junctions containing islands larger than d_{cr} will approach the limit of parallel diodes, in which their *I-V* characteristics are dominated by the lower LBH islands as summarized in Fig. 5. Substituting the experimental values of $\Phi_B = 1.35$ eV, $W = 121$ nm, $\Delta = 1.0$ eV for 1 uc of $LaAlO_3$, we obtain $d_{cr} = 90$ nm, which lies between the island sizes directly observed by AFM in Figs. 2(a) and (d).

In summary, we have studied the effect of fractional coverage of a $LaAlO_3$ interface dipole on the macroscopic junction properties in $SrRuO_3$/Nb:$SrTiO_3$ (001) Schottky junctions. Atomic scale $LaAlO_3$ dipole layers with fractional coverage were inserted at the interface to locally form reduced LBH regions. By increasing the lateral size of these low LBH regions, the *I-V* characteristics transformed from a rectifying diode with an area-weighted average SBH to a more conductive junction dominated by

the low LBH. The estimated threshold separating the two regimes was well explained by considering the electrostatic landscape induced by the LBH inhomogeneity. While there have been a series of studies about inhomogeneous Schottky junctions in the past,[25-27] and more recently applied to Schottky junctions incorporating nanostructures,[28-30] here we experimentally analyzed the macroscopic band bending at the fully epitaxial interface, minimizing the extrinsic effects from imperfections which often obscure the analyses at more complex interfaces. These results present guidelines to control band alignments on the scale of 10-100 meV using oxide dipoles and should be effective in applications such as hot electron spectroscopy in the metal-base-transistor geometry,[31] as well as photoelectrochemical applications in which the potential landscape critically impacts the efficiency of the charge transfer across the semiconductor interfaces.[10, 32, 33]

ACKNOWLEDGMENTS

This work was supported by the Department of Energy, Office of Basic Energy Sciences, Division of Materials Sciences and Engineering under Contract No. DE-AC02-76SF00515.

REFERENCES

[1] R. Ramesh and D. Schlom, MRS Bulletin **33**, 1006 (2008).

[2] K. Hashimoto, H. Irie, and A. Fujishima, Jpn. J. Appl. Phys. **44**, 8269 (2005).

[3] G. H. Haertling, J. Am. Ceram. Soc. **82**, 797 (1997).

[4] H. Ohta and H. Hosono, Materials Today **7**, 42 (2004).

[5] R. L. Anderson, Solid-State Elec. **5**, 341 (1962).

[6] Y. Hikita, M. Nishikawa, T. Yajima, and H. Y. Hwang, Phys. Rev. B **79**, 073101 (2009).

[7] T. Yajima, Y. Hikita, M. Minohara, C. Bell, J. A. Mundy, L. F. Kourkoutis, D. A. Muller, H. Kumigashira, M. Oshima, and H. Y. Hwang, Nature Commun. **6**, 6759 (2015).

[8] T. Yajima, M. Minohara, C. Bell, H. Kumigashira, M. Oshima, H. Y. Hwang, and Y. Hikita, Nano Lett. **15**, 1622 (2015).

[9] T. Tachikawa, M. Minohara, Y. Hikita, C. Bell, and H. Y. Hwang, Adv. Mater. **27**, 7458 (2015).

[10] Y. Hikita, K. Nishio, L. C. Seitz, P. Chakthranont, T. Tachikawa, T. F. Jaramillo, and H. Y. Hwang, Adv. Energy Mater. **6**, 1502154 (2016).

[11] Z. Zhong and P. Hansmann, Phys. Rev. B **93**, 235116 (2016).

[12] T. Tachikawa, H. Y. Hwang, and Y. Hikita, Appl. Phys. Lett. **111**, 091602 (2017).

[13] J. M. Shannon, Solid-State Electronics **19**, 537 (1976).

[14] C. C. Han, E. D. Marchall, F. Fang, L. C. Wang, and S. S. Lau, J. Vac. Sci. Technol. B **6**, 1662 (1998).

[15] H. Inoue, A. G. Swartz, N. J. Harmon, T. Tachikawa, Y. Hikita, M. E. Flatté, and H. Y. Hwang, Phys. Rev. X **5**, 041023 (2015).

[16] A. G. Swartz, H. Inoue, T. A. Merz, Y. Hikita, S. Raghu, T. P. Devereaux, S. Johnston, and H. Y. Hwang, Proc. Natl. Acad. Sci. U. S. A. **115**, 1475 (2018).

[17] M. Minohara, I. Ohkubo, H. Kumigashira, and M. Oshima, Appl. Phys. Lett. **90**, 132123 (2007).

[18] Y. Hikita, Y. Kozuka, T. Susaki, H. Takagi, and H. Y. Hwang, Appl. Phys. Lett. **90**, 143507 (2007).

[19] R. T. Tung, Appl. Phys. Lett. **58**, 2821 (1991).

[20] M. Lippmaa, N. Nakagawa, and M. Kawasaki, Appl. Phys. Lett. **74**, 3543 (1999).

[21] G. Koster, B. L. Kropman, G. J. H. M. Rijnders, D. H. A. Blank, and H. Rogalla, Appl. Phys. Lett. **73**, 2920 (2011).

[22] S. M. Sze and K. K. Ng, Physics of Semiconductor Devices 3rd edn (John Wiley, 2007).

[23] I. Ohdomari and K. N. Tu, J. Appl. Phys. **51**, 3735 (1980).

[24] Z. Sroubek, Phys. Rev.B **2**, 3170 (1970).

[25] A. Olbrich, J. Vancea, F. Kreupl, and H. Hoffmann, J. Appl. Phys. **83**, 358 (1998).

[26] H.-J. Im, Y. Ding, J. P. Pelz, and W. J. Choyke, Phys. Rev. B **64**, 075310 (2001).

[27] H. Haick, M. Ambrico, T. Ligonzo, R. T. Tung, and D. Chaen, J. Am. Chem. Soc. **128**, 6854 (2006).

[28] M. S. Gorji and K. Y. Cheong, Crit. Rev. Solid Stat. and Mater. Sci. **40**, 197 (2015).

[29] M. D. Tomer, S. Rajput, and L. Li, J. Phys. D: Appl. Phys. **50**, 165301 (2017).

[30] C. A. Amorim, E. P. Bernardo, E. R. Leite, and A. J. Chiquito, Semicond. Sci. Technol. **33**, 055003 (2018).

[31] T. Yajima, Y. Hikita, and H. Y. Hwang, Nature Mater. **10**, 198 (2011).

[32] R. C. Rossi and N. S. Lewis, J. Phys. Chem. B **105**, 12303 (2001).

[33] A. T. Garcia-Esparza and K. Takanabe, J. Mater. Chem. A **4**, 2894 (2016).

FIG. 1. (a,b) Schematic illustrations of $SrRuO_3$/Nb:$SrTiO_3$ (001) Schottky junctions with (a) integer and (b) fractional $LaAlO_3$ dipole layer insertion.

FIG. 2. (a-e) AFM images of the 0.4 uc $LaAlO_3$ layer deposited on the Nb:$SrTiO_3$ (001) substrate at various temperatures: (a) 750 ºC, (b) 850 ºC, (c) 950 ºC, and (d) 1100 ºC. (e) Friction force microscopy (FFM) image corresponding to (d).

FIG. 3. (a,b) *I-V* characteristics of $SrRuO_3$/Nb:$SrTiO_3$ (001) Schottky junctions with varied thickness of the $(AlO_2)^-/(LaO)^+$ dipole layer grown at (a) 750 ºC and (b) 1100 ºC.

FIG. 4. (a) The measured Schottky barrier heights versus the thickness of the $LaAlO_3$ (T_s = 750 ºC). The dashed curve shows the calculated SBH based on the parallel-diode model for the $LaAlO_3$ dipole, and the dotted line shows the $\overline{\Phi}_B^A$ with $\Phi_B = 1.35$ eV and $\Delta = 1.0$ eV. (b) Simulated potential landscape along the in-plane direction (x) and the out-of-plane direction (z) within the range $0 < x < W$. The inset shows the dipole island distribution used for the simulation, corresponding to ~18 % areal coverage, and the dashed line indicates the position of the cross section corresponding to the simulated potential. (c) The measured ideality factors versus the dipole coverage. (d) The calculated *I-V* characteristics of $SrRuO_3$/Nb:$SrTiO_3$ (001) Schottky junctions with varied thickness of the $(AlO_2)^-/(LaO)^+$ dipole layer.

FIG. 5. Schematic illustration comparing the island size and the threshold crossover from the electrically homogeneous (Schottky) regime to the parallel-diode (leakage) regime.

(a)
$LaAlO_3$
+
–
$SrRuO_3$
Nb:$SrTiO_3$
(b)
$LaAlO_3$ (fractional)
$SrRuO_3$
Nb:$SrTiO_3$

(a) 750 ℃

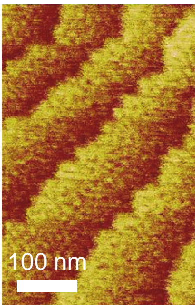

(b) 850 ℃

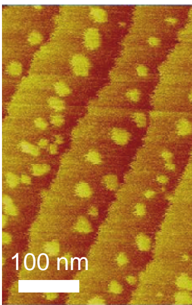

(c) 950 ℃

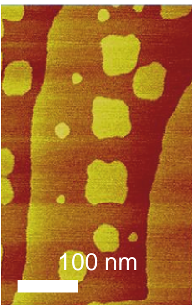

(d)1100 ℃

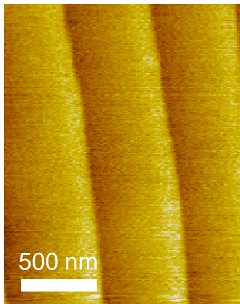

(e) 1100 ℃ (FFM)

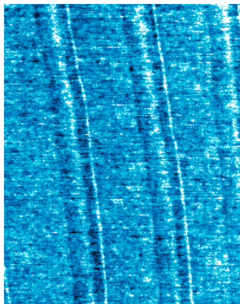

(a) 750 ℃
(b) 1100 ℃
10^{-1}
10^{-2}
10^{-3}
10^{-4}
10^{-5}
10^{-6}
10^{-7}
10^{-8}
10^{-9}
| I | (A)
-1
0
1
V (V)
$LaAlO_3$ (uc)
2.0
1.0
0.8
0.6
0.4
0.2
0.0
$LaAlO_3$ (uc)
2.0
1.6
1.3
0.9
0.6
0.2
0.0

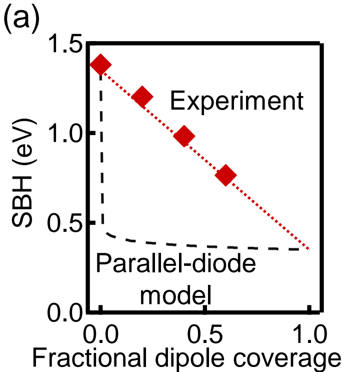

(b)
Dipole islands
d = 10 nm
Φ_B
$\overline{\Phi}_B^A$
1.0
Electron energy (eV)
$\Phi_B-\Delta$
$SrRuO_3$
$Nb:SrTiO_3$
0
z (nm)
50
0
50
100
x (nm)
y
x

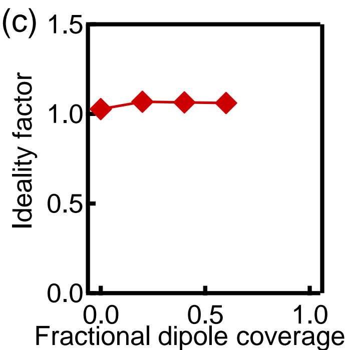

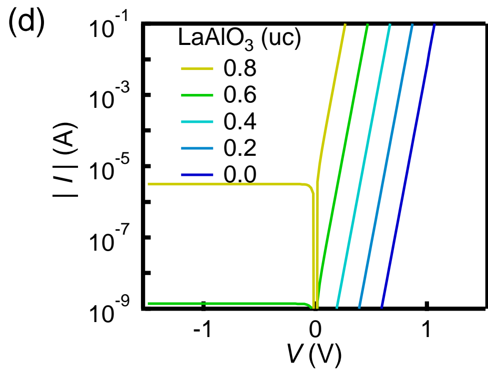

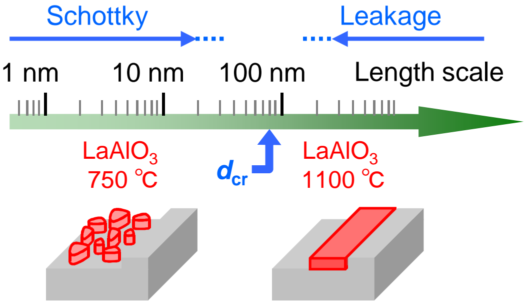
Schottky
Leakage
1 nm
10 nm
100 nm
Length scale
LaAlO3
750 ℃
d_cr
LaAlO3
1100 ℃